Effect of Water and DMSO on Mechanoelectrical Conversion of Schottky DC Generators

Xiang Ding[a], Hao Shao[a], Hongxia Wang[a], Ruixi Bai[a], Jian Fang[b], Tong Lin[c]*

a Institute for Frontier Materials, Deakin University, Geelong, VIC 3216, Australia
b College of Textile and Clothing Engineering, Soochow University, Suzhou, 215123, China
c State Key Laboratory of Separation Membranes and Membrane Processes, School of Textile Science and Engineering, Tiangong University, Tianjin 300387, China

* Corresponding author's email: tong.lin@tiangong.edu.cn

Electronic Supplementary Information

Table S1. Summary of various Schottky DC energy generators

Types	Active layers	Peak voltage (V)	Current Density ($\mu A\ cm^{-2}$)	Refs
Schottky diode/p-n junction (Sliding mode)	Al tip/n-type Si	0.60	4000	1
	Graphene/n-type Si	0.22	1.5	1
	ITO/n-type Si	0.45	2.5	1
	Al/n-type Si	0.60	4	1
	Graphene/n-GaAs	0.12	0.14	1
	ITO/n-GaAs	0.23	0.25	1
	Al/n-GaAs	0.48	4.1	1
	n-GaAs/SiO_2/p-Si	3.1	100	2
	MoS_2/AlN/Si	5.1	11200	2
	p-Si/n-GaAs	0.7	180	2
	Pt/Ir-coated nano-sized tip on MoS_2	0.007	10^8	3
	C-AFM tip/InP	-	$2.3*10^5$	4
	C-AFM tip/Si	-	$2.9*10^7$	5
	Carbon aerogel/Si	2	20	6
	n-type Si/p-type Si	0.31	$5.8*10^{-2}$	7
	Au tip/ p-Si	0.32	3500	8

Schottky diode/p-n junction (Compression mode)	Al/PPy/Au	0.70	62.4	9
	Al/PEDOT/Au	0.87	49.0	9
	Al/PANI/Au	1.0	33.6	9
	Al/PPy/SnO_2/Au	0.25	2.7	10
	Al/SnO_2/Au	0.08	0.38	10
	Al/PPy/Al_2O_3/Au	0.006	0.004	10
	Al/PPy/ZnO/Au	0.019	0.013	10
	Al/PANI/SnO_2/Au	0.14	0.47	10
	Al/PEDOT/SnO_2/Au	0.10	1.28	10
	Al/PANI/Au (doped with HCl)	0.9	33.9	10
	Al/PPy-GO/Au (doped with 1.6 wt% GO)	0.73	131.9	11
	Al/PPy-TiO_2/Au (doped with 11.35 wt% TiO_2)	0.84	431.47	12
	Al/PPy/Au (containing 10.49 wt% water)	**1.01**	**197.84**	**This work**
	Al/PPy/Au (doped with 0.66 wt% DMSO)	**0.95**	**222.35**	**This work**

Table S2. Effect of moisture on the electrical output of nanogenerators

Nanogenerator type	Relative humidity (%)	Effect	Open-circuit voltage (V)	Short-circuit current (µA)	Device structure (active layer)	Ref
Triboelectric nanogenerator (contact-separation mode)	95	Positive effect	695.18	29.72	PTFE/PVA	13
	95	Positive effect	330	16.6	Starch biofilm/PTFE	14
	90	Positive effect	664	37	PVDF/PVA-LiCl film	15
	90	Negative effect	67.5	13.9	PANI-Poly (ethylene-co-poly (vinyl alcohol)) composite nanofiber membranes/PTFE	16
	90	Negative effect	42	2.95	Cellulose acetate/Polyurethane-NH_2 nanofiber membranes/PVDF	17
	80	Negative effect	130	15	Chitosan-glycerol film/PTFE	18
	100	Negative effect	18	0.5	PTFE/FTO glass	19
	99	Negative effect	14	3.7	Polyimide/GO paper	20
Triboelectric nanogenerator (sliding mode)	60	Positive effect	1.3	30.3	Al/ asymmetric graphene oxide /Al	21
	90	Negative effect	26	0.4	Polyimide film/Cu foil	22
Piezoelectric nanogenerator	60	Negative effect	0.05	-	Al/Al-doped ZnO nanowire arrays/Ti	23
	60	Negative effect	0.21	-	Al/Fe-doped ZnO nanowire arrays/Ti	24

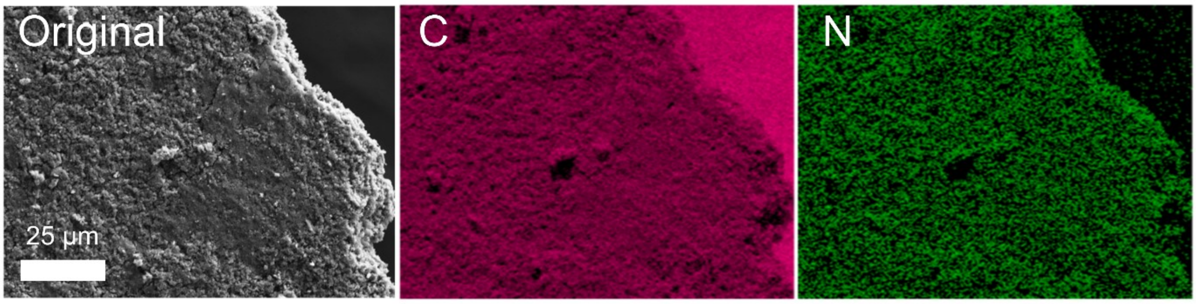

Fig. S1 SEM image and EDS mapping of elements C and N in polypyrrole. The upper right corner of EDS mapping of C is ascribed to adhesive carbon tape.

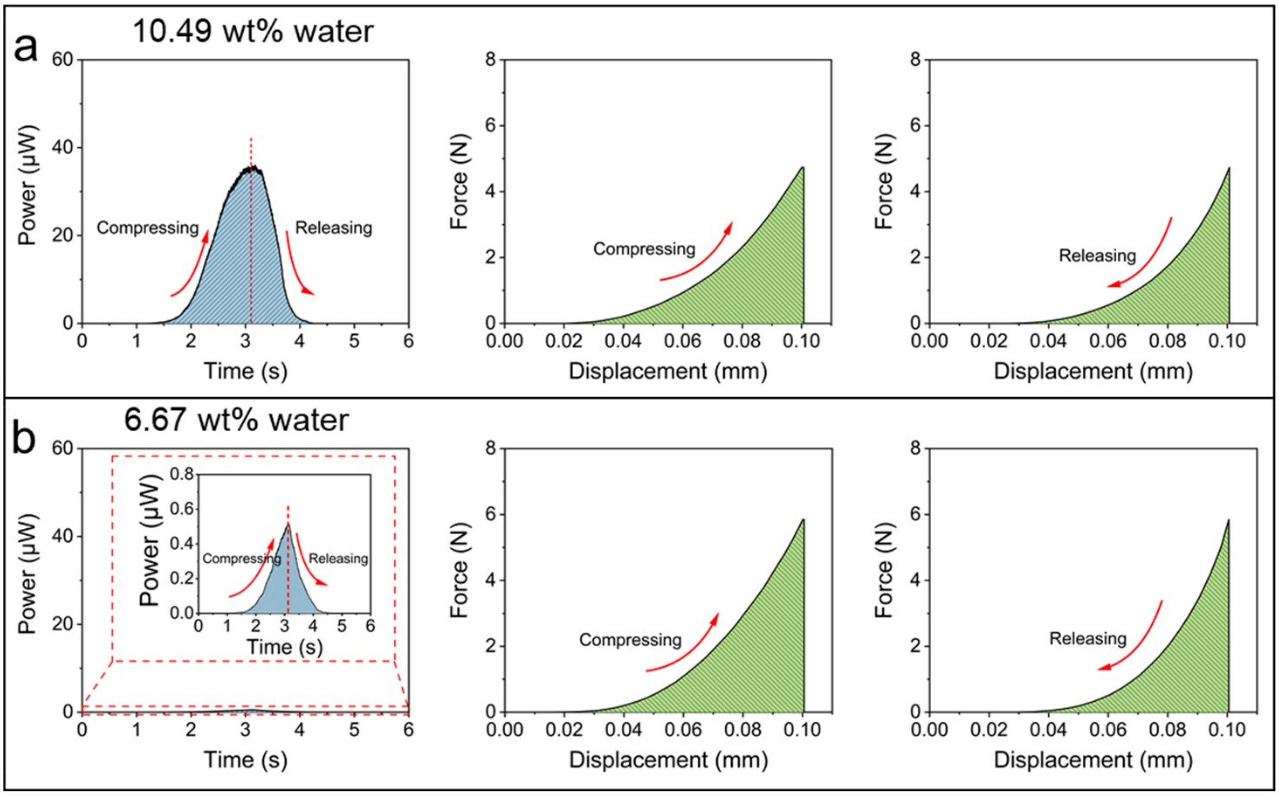

Fig. S2 The power outputs and force-displacement curves of Schottky devices made of (a) PPy containing 10.49 wt% water (external resistor 5.6 kΩ) and (b) PPy containing 6.67 wt% water (external resistor 130 kΩ) device under one compression and decompression cycle (strain: 6%, compressing & releasing speed: 0.035 mm s^{-1}).

Schottky devices were connected with a resistor that matched the internal resistance to obtain the maximum output power. According to I-t curves, P-t curves can be obtained, as shown in Fig. S2. The electrical output can be calculated through the integral area under the P-t curve, using the equation:

$$E_{electrical} = \int P\,dt = \int I(t)^2 R\,dt \qquad (1)$$

For the PPy containing 10.49 wt% water, one-cycle power was calculated as 4.36×10^{-5} J when (from the average of over eight cycles).

The force-displacement curve (Fig. S2a) can be obtained from Instron Tensile Tester. The work of force can be calculated by the integral of the F-S curve. For the PPy containing 10.49 wt% water, the one-cycle of input mechanical energy calculated based on Fig. S2a was 2.05×10^{-4} J.

Thus, the energy conversion efficiency of the Schottky DC generator can be estimated by the equation:

$$\eta = \frac{E_{electrical}}{E_{mechanical}} = \frac{\int P\,dt}{\int F(s)\,ds} = \frac{\int I(t)^2 R\,dt}{\int F(s)\,ds} \qquad (2)$$

For the PPy device with high water content (10.49 wt%) under 6.0% strain, the device efficiency was 21.27%, which is over 90 times higher than that of the device with 6.67 wt% water content (0.22%, Fig. S2b).

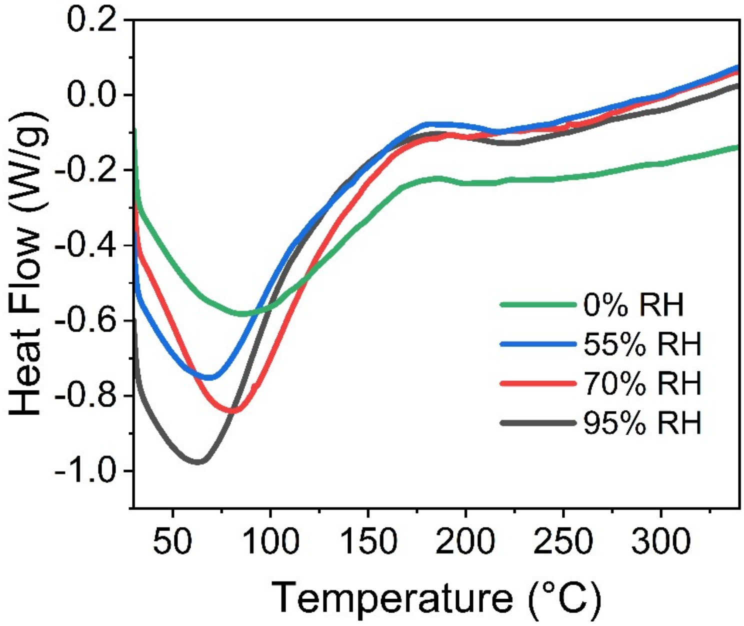

Fig. S3 DSC curves for polypyrrole samples stored in different humidity environments.

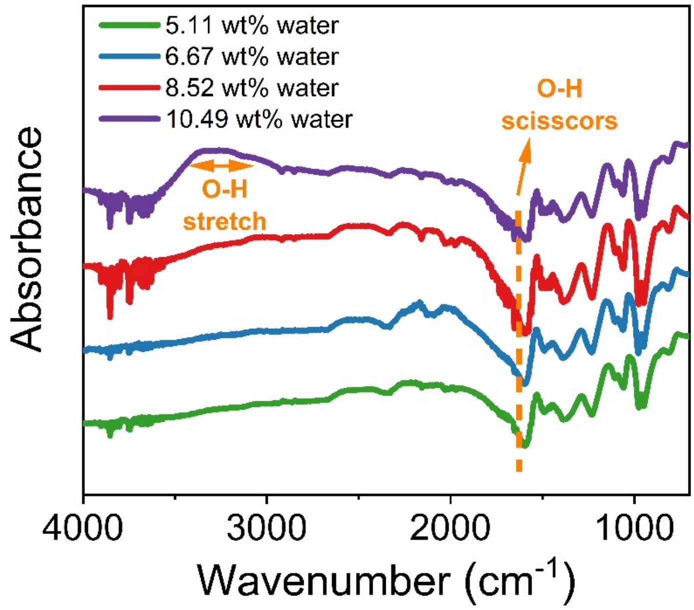

Fig. S4 FITR spectra for polypyrrole samples stored in different humidity environments.

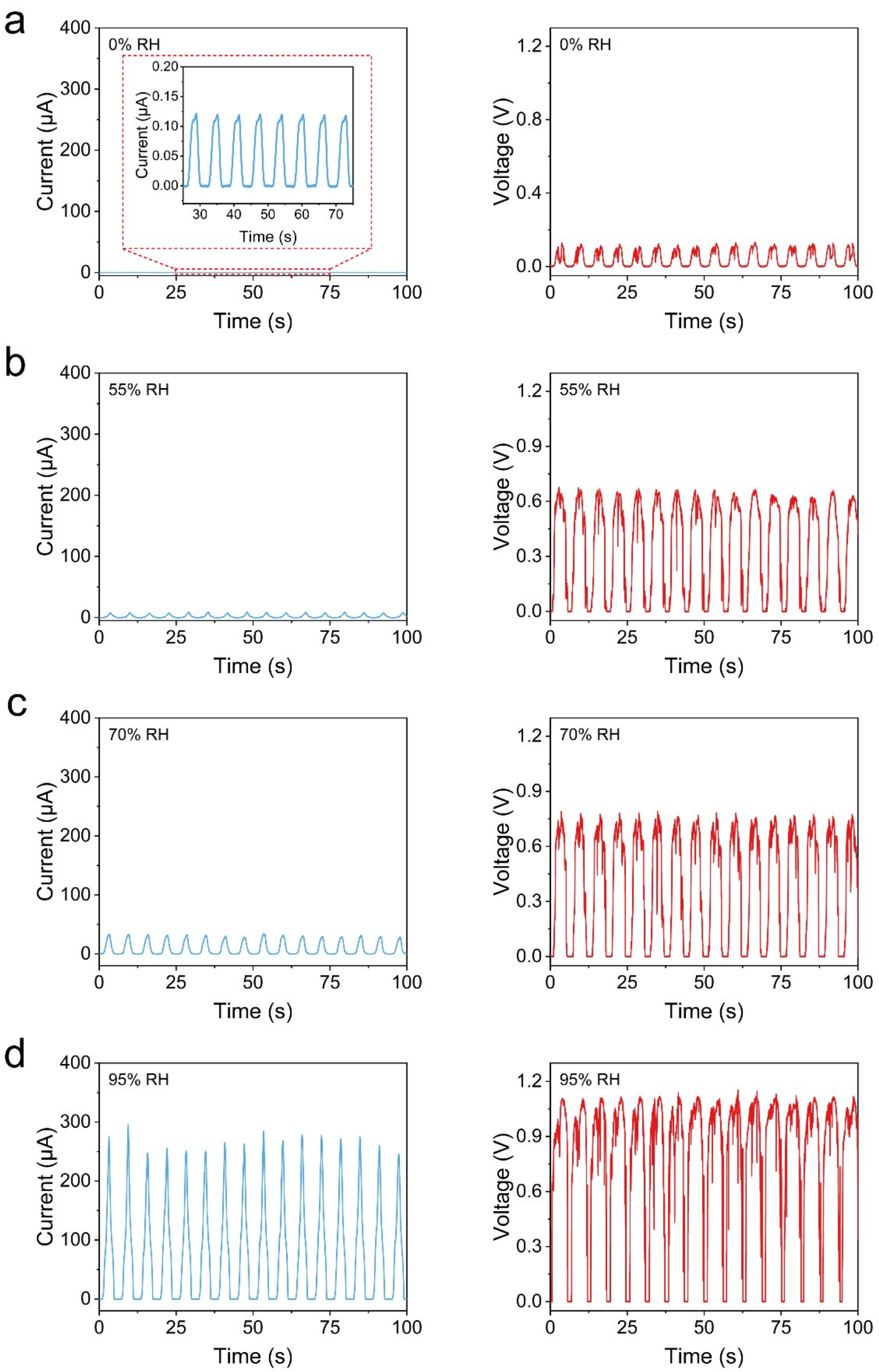

Fig. S5 Current and voltage outputs of the PPy based Schottky devices stored in (a) 0% RH, (b) 55% RH, (c) 70% RH and (d) 95% RH (strain: 6%, compressing & releasing speed: 0.035mm s^{-1}, temperature: 20 °C).

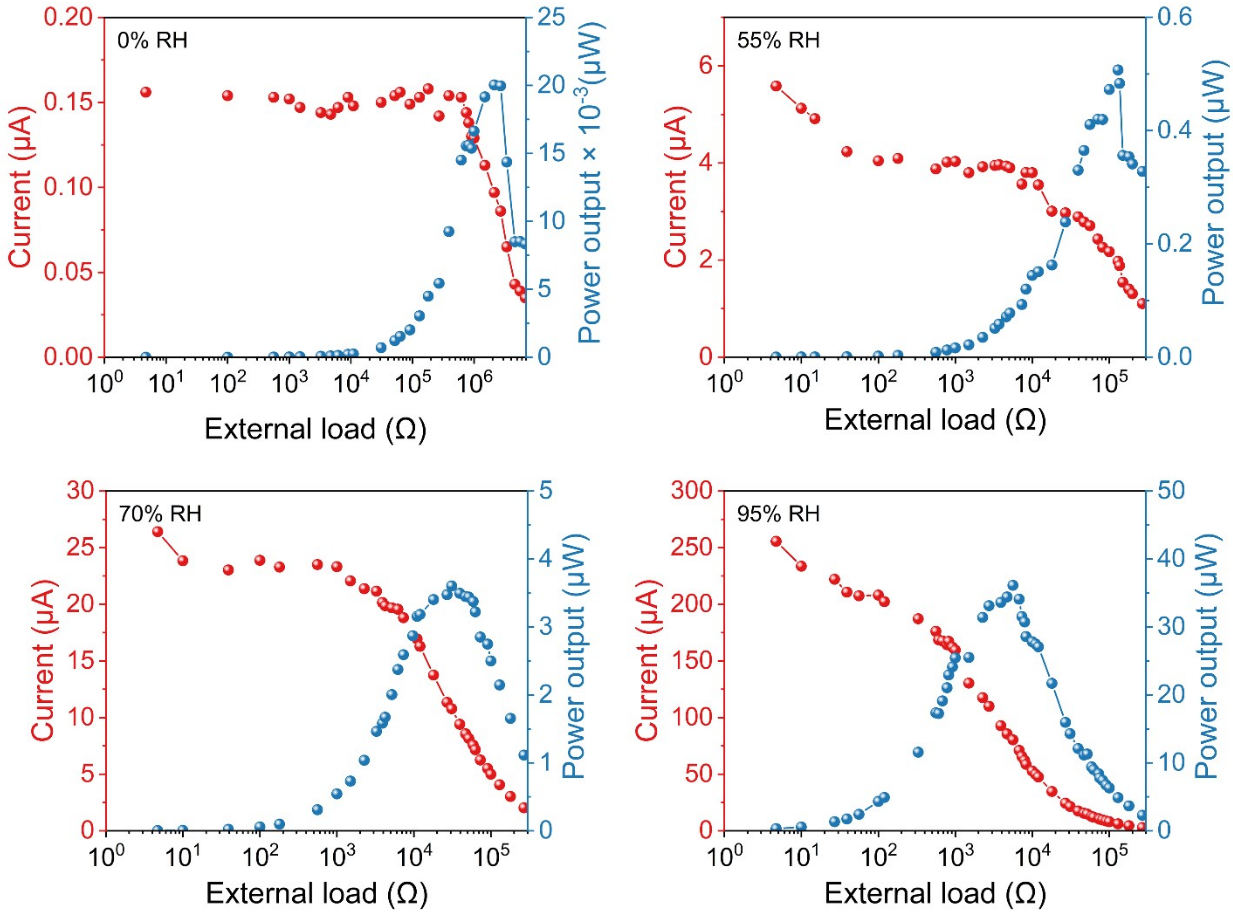

Fig. S6 Dependency of the current and power outputs on external resistances for PPy-based Schottky devices stored in different humidity environments.

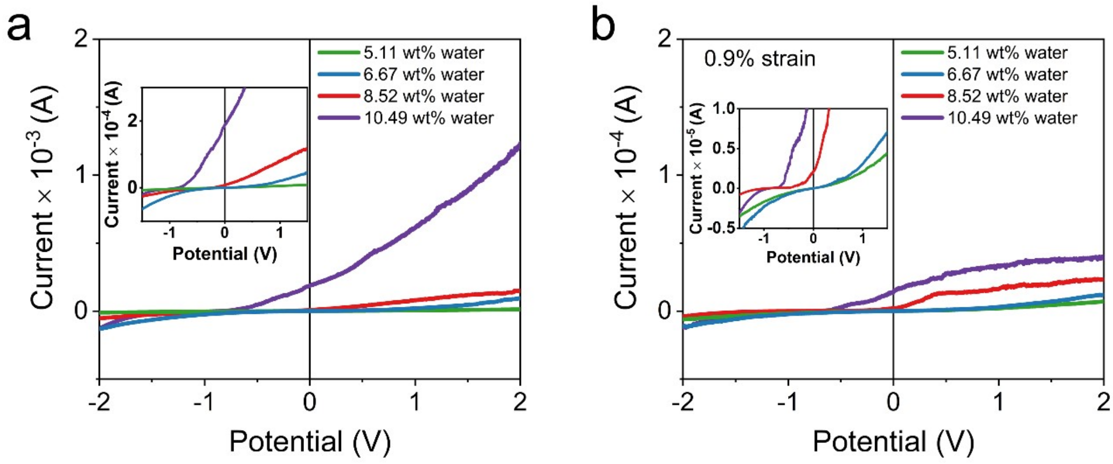

Fig. S7 I–V characteristics of the Schottky DC generators with different water content at (a) 6.0% strain and (b) 0.9% strain (inset: enlarge the display of the curves around the null point).

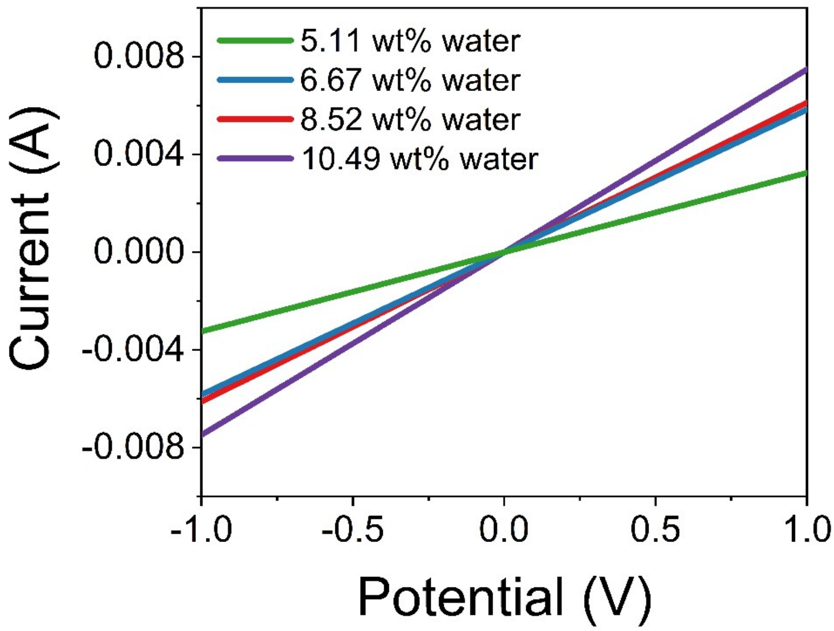

Fig. S8 I–V characteristics of the Au/PPy-water/Au devices at the strain level of 6.0%.

We measured the resistance of the PPy device by sandwiching the PPy disc with two Au electrodes in between. The IV curve had a linear relationship because of the ohmic contact between PPy and Au. Based on the slope, the resistance in the thickness direction can be estimated. At 6.0% strain, the resistance values are 307.69 Ω, 171.23 Ω, 163.40 Ω, and 133.69 Ω for the PPy discs containing 5.11 wt%, 6.67 wt%, 8.52 wt%, and 10.49 wt% water, respectively.

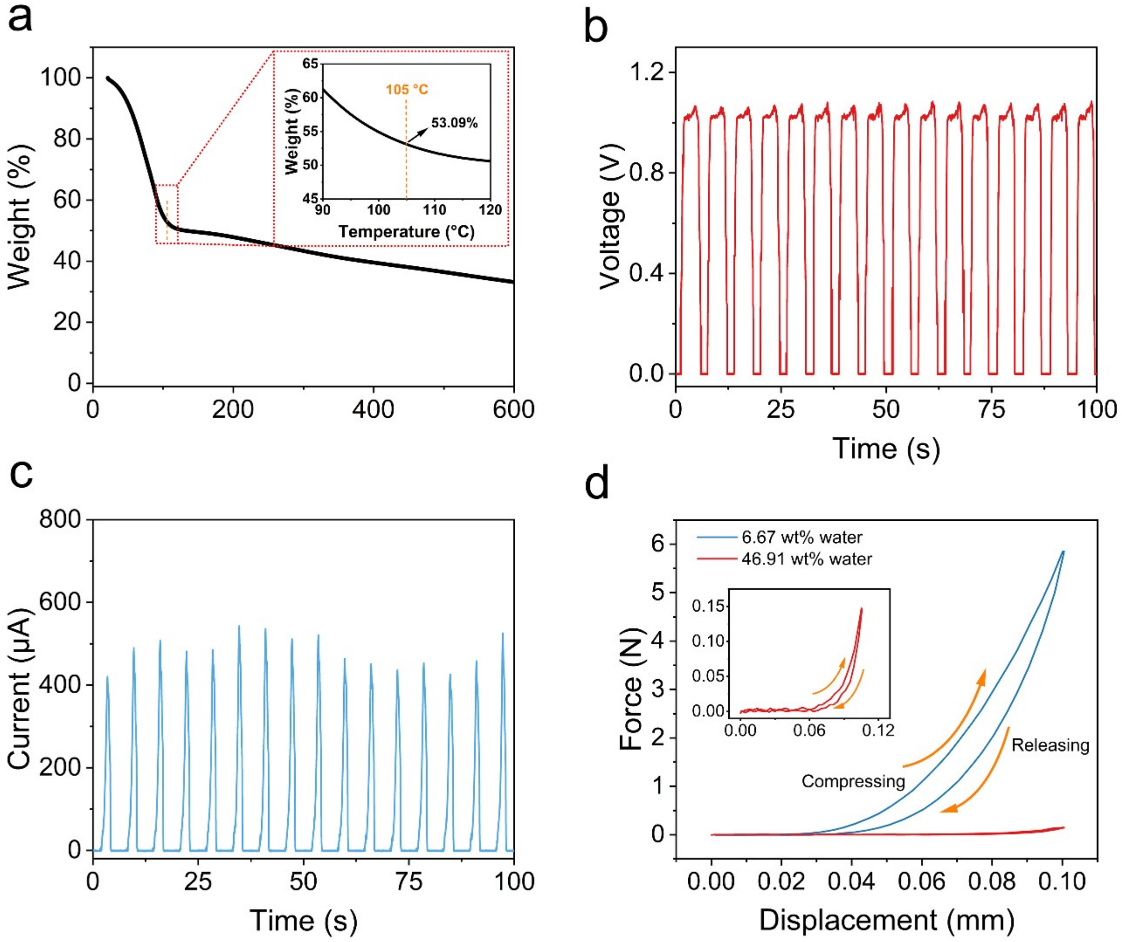

Fig. S9 (a) TGA curve of PPy samples wrapped with wet tissues. (b) V_{oc} and (c) I_{sc} of the Schottky device (strain: 6.0%, compressing & releasing speed: 0.035mm s^{-1}). (d) Force-displacement curves of PPy disc (inset: enlarged the display the curve of PPy containing 46.91wt% water)

The PPy discs were wrapped with well-wet tissues and kept at 20 °C for 5 hours to obtain samples with high water content. The water content estimated based on the TGA curve was 46.91 wt%. Fig. S9b and S9c show the Voc and Isc of the device. The open-circuit voltage reached 1.07 ± 0.07 V, and the short-circuit current outputs were as high as 485.06 ± 72.63 μA. However, the excess water content made the polypyrrole plate lose its mechanical properties, as shown in Fig. S9d.

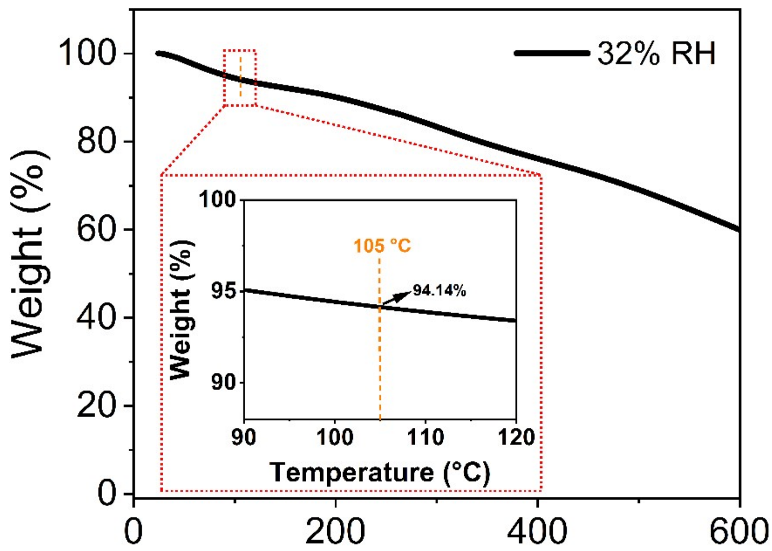

Fig. S10 TGA curve of PPy sample kept in 32% RH.

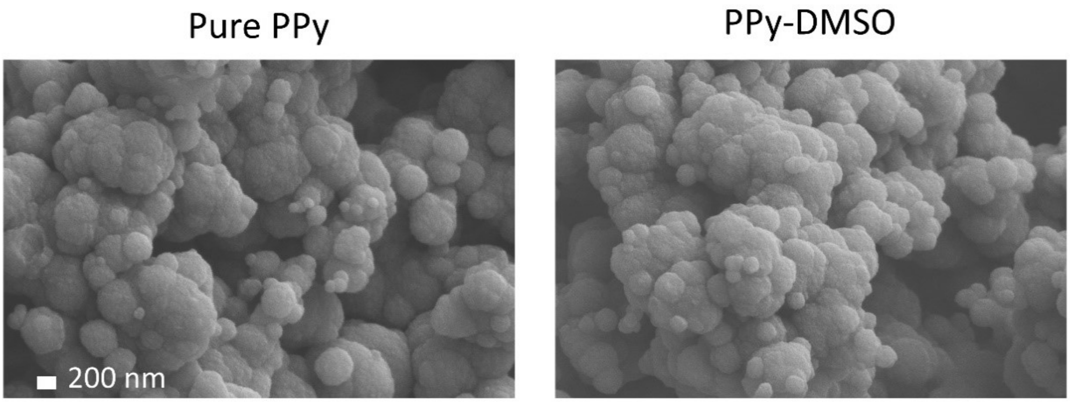

Fig. S11 SEM images of pure PPy and PPy-DMSO (DMSO content: 15 wt%).

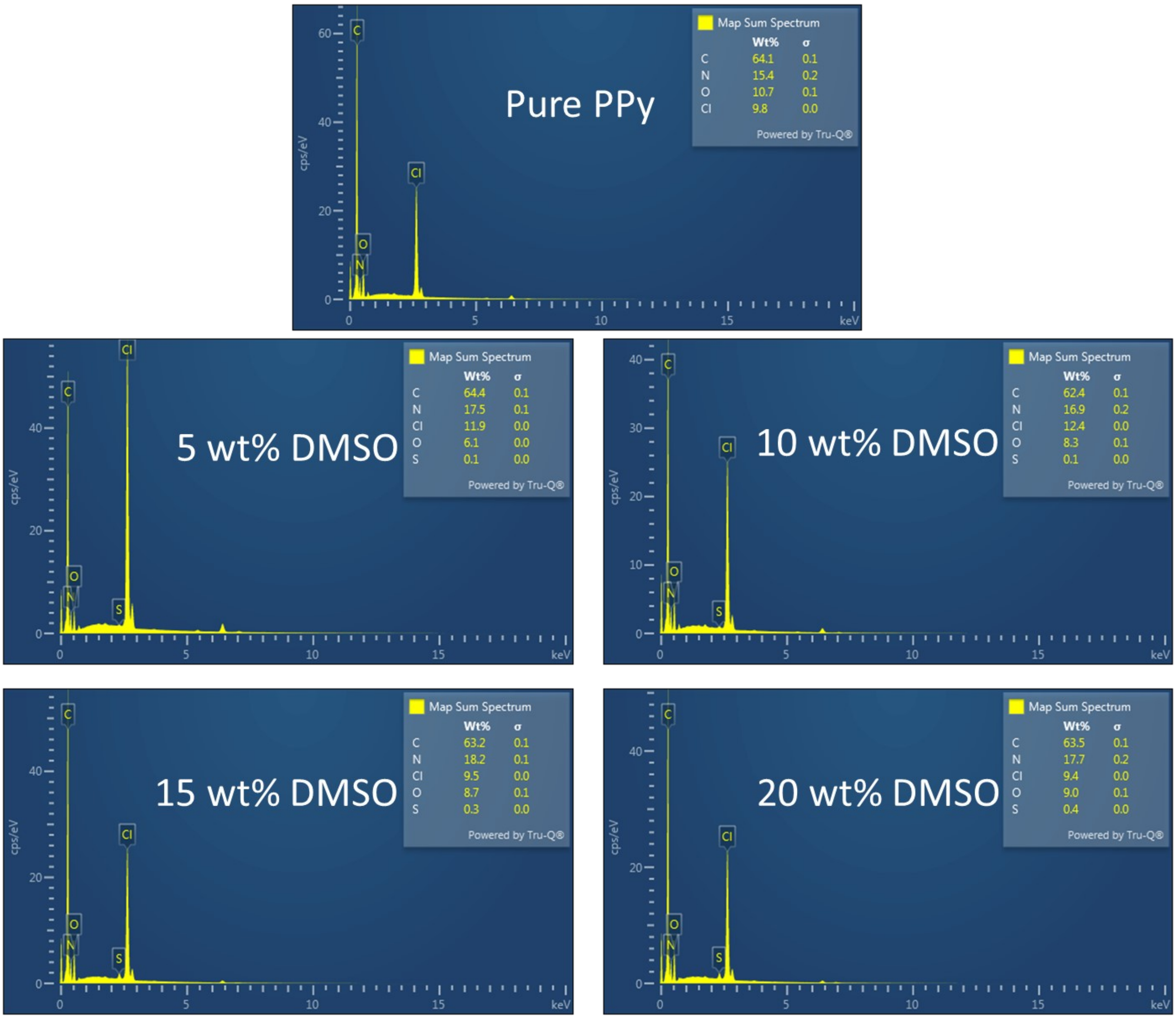

Fig. S12 EDX spectrum of PPy and PPy-DMSO samples.

Table S3. EDS element S quantification results.

Samples	DMSO in the reaction solution (wt% based on pyrrole)	Sulfur (wt%)	DMSO content in polypyrrole (wt%)
PPy	0	0	0
PPy-DMSO	5	0.06	0.15
	10	0.18	0.44
	15	0.27	0.66
	20	0.36	0.88

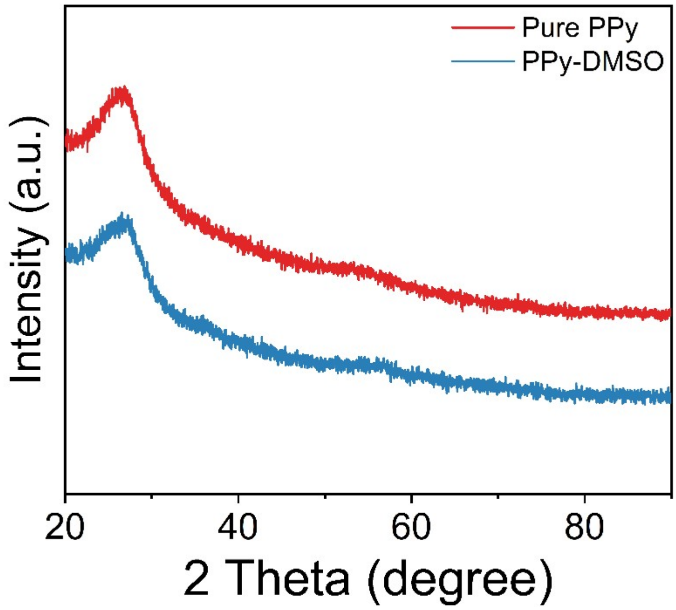

Fig. S13 XRD patterns of PPy and PPy-DMSO (DMSO content: 0.66 wt%).

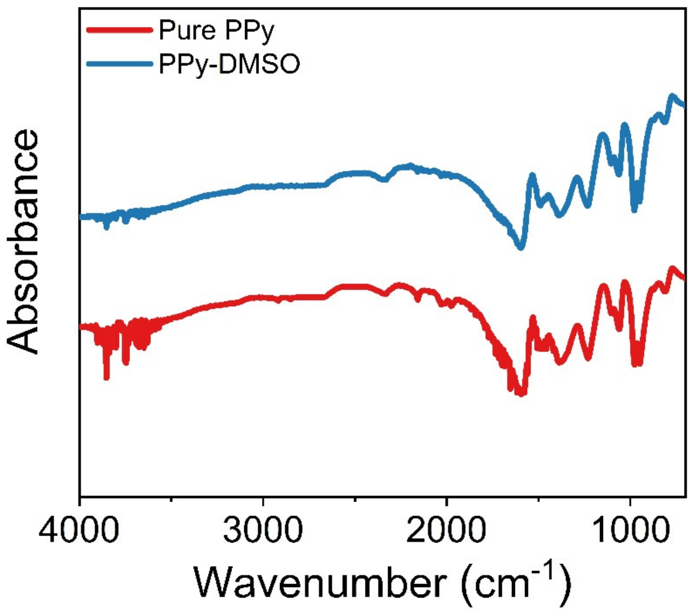

Fig. S14 FTIR spectra of pure PPy and PPy-DMSO (DMSO content: 0.66 wt%).

Fig. S14 shows the FTIR spectra of PPy and PPy-DMSO. The characteristic peaks at 771 cm^{-1} correspond to C–H stretching, whereas bands at 1022 and 1087 cm^{-1} were assigned to =C–H in-plane deformation vibration. The peaks at 1147 cm^{-1} corresponded to C–H in and out of plane deformations[9,11,12].

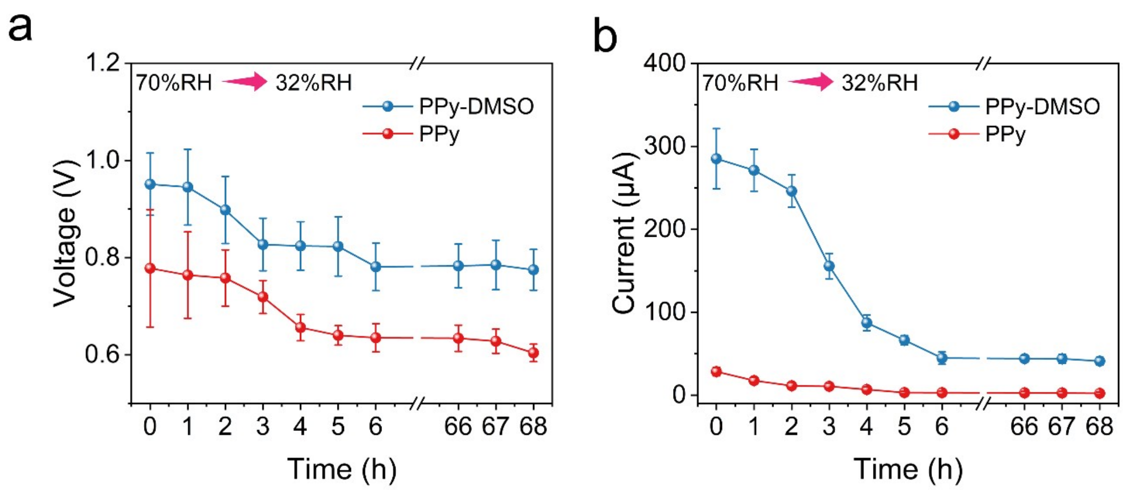

Fig. S15 Changes in (a) voltage and (b) current outputs when the devices conditioned in 70% RH were transferred from a 32% RH environment.

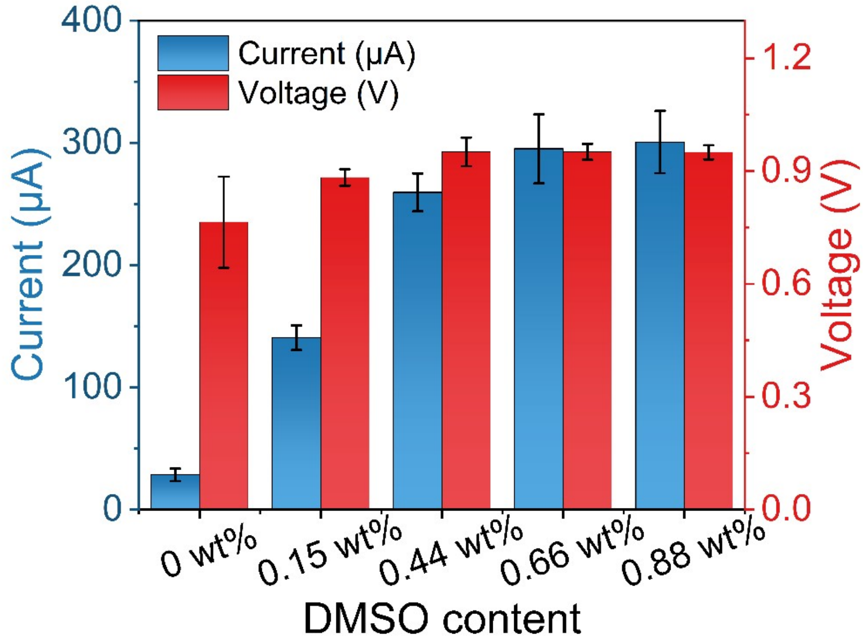

Fig. S16 Effect of DMSO content on electrical outputs of the PPy-DMSO devices with different DMSO contents in PPy (strain 6%, compressing & releasing speed: 0.035mm s^{-1}, relative humidity: 70% RH, temperature: 20 °C).

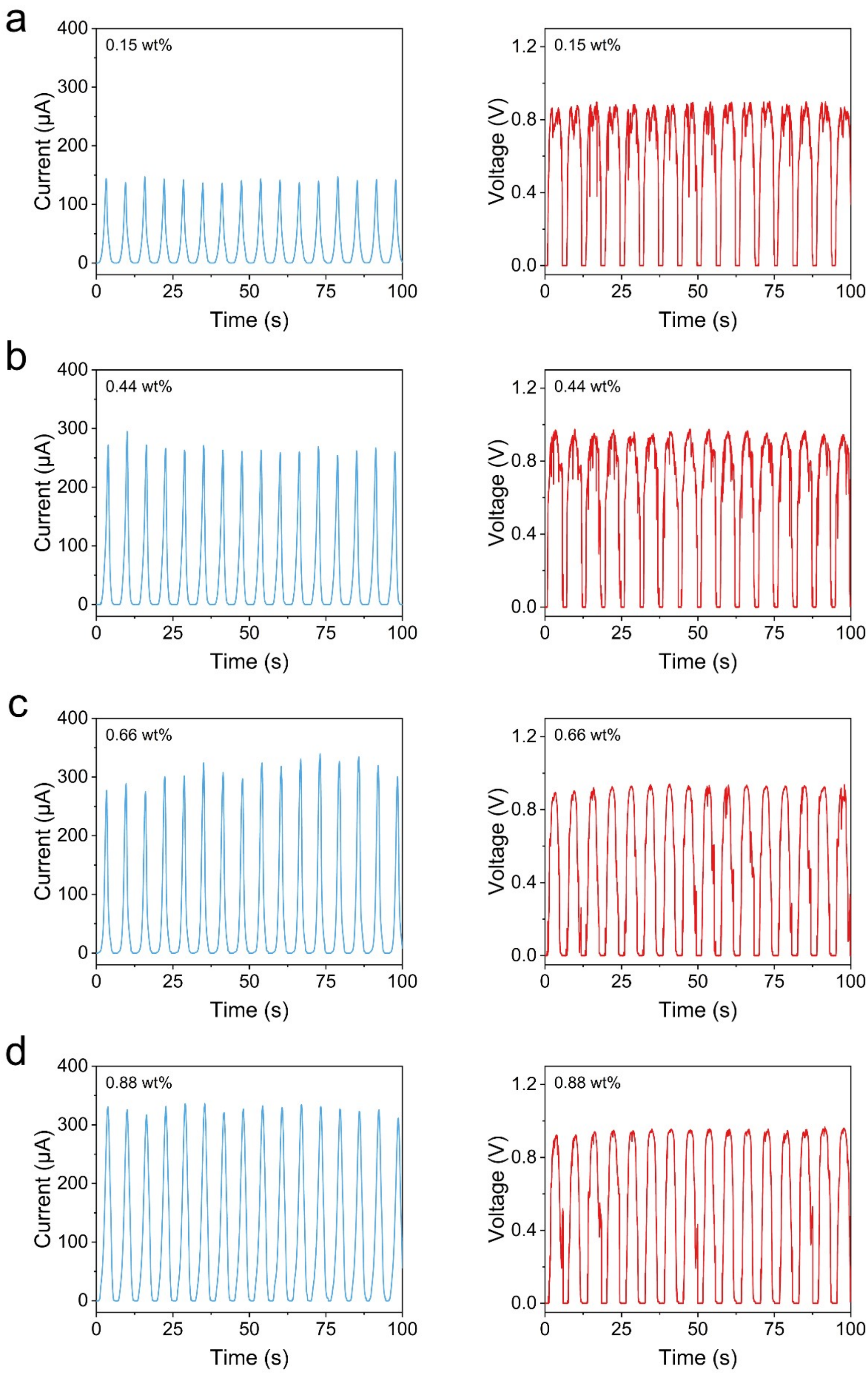

Fig. S17 Short-circuit current and open-circuit voltage of PPy-DMSO devices with different DMSO contents in PPy: (a) 0.15 wt%, (b) 0.44 wt%, (c) 0.66 wt%, (d) 0.88 wt% (strain 6%, compressing & releasing speed: 0.035mm s^{-1}, relative humidity: 70% RH, temperature: 20 °C).

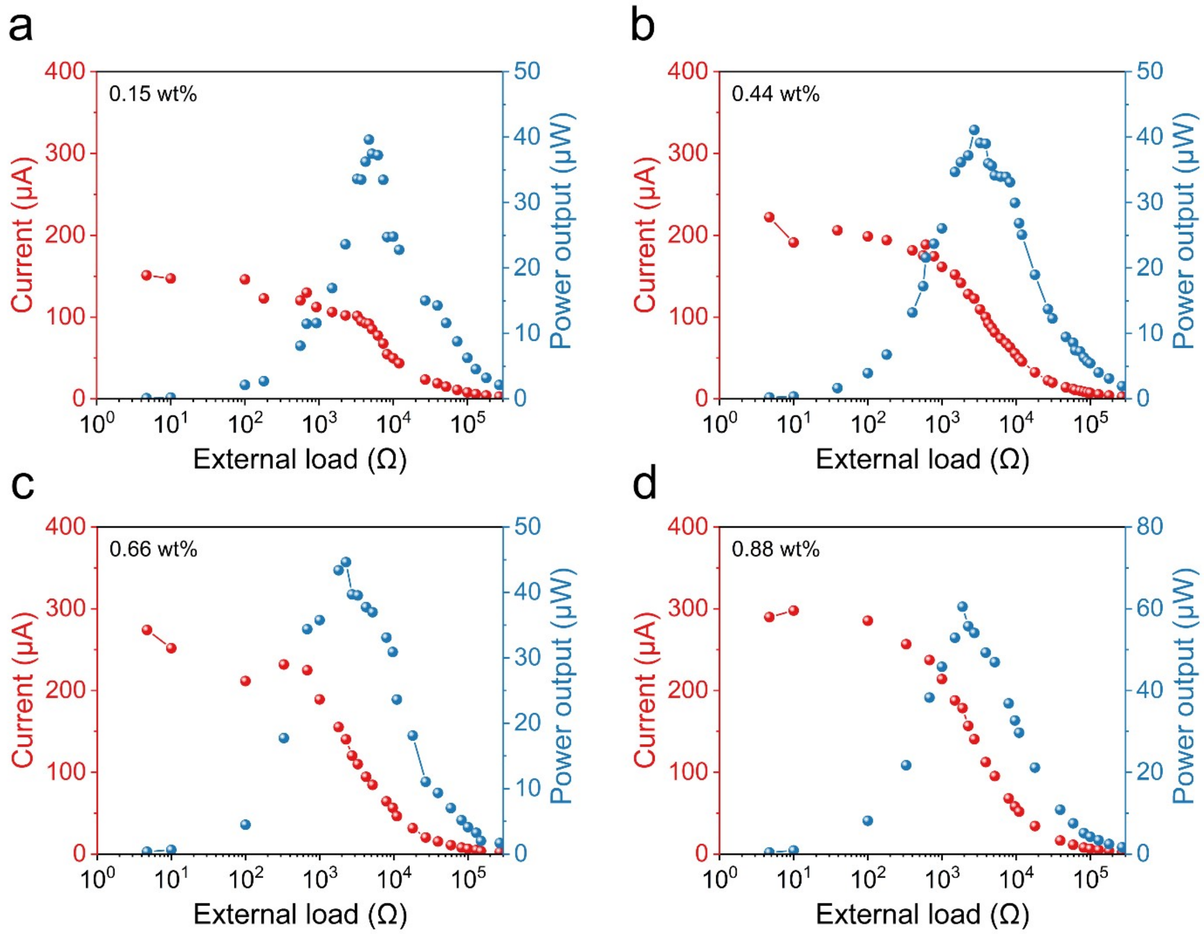

Fig. S18 Dependency of the current and power outputs on external resistances for PPy-DMSO devices with DMSO content of (a) 0.15 wt%, (b) 0.44 wt%, (c) 0.66 wt%, (d) 0.88 wt% in the PPys.

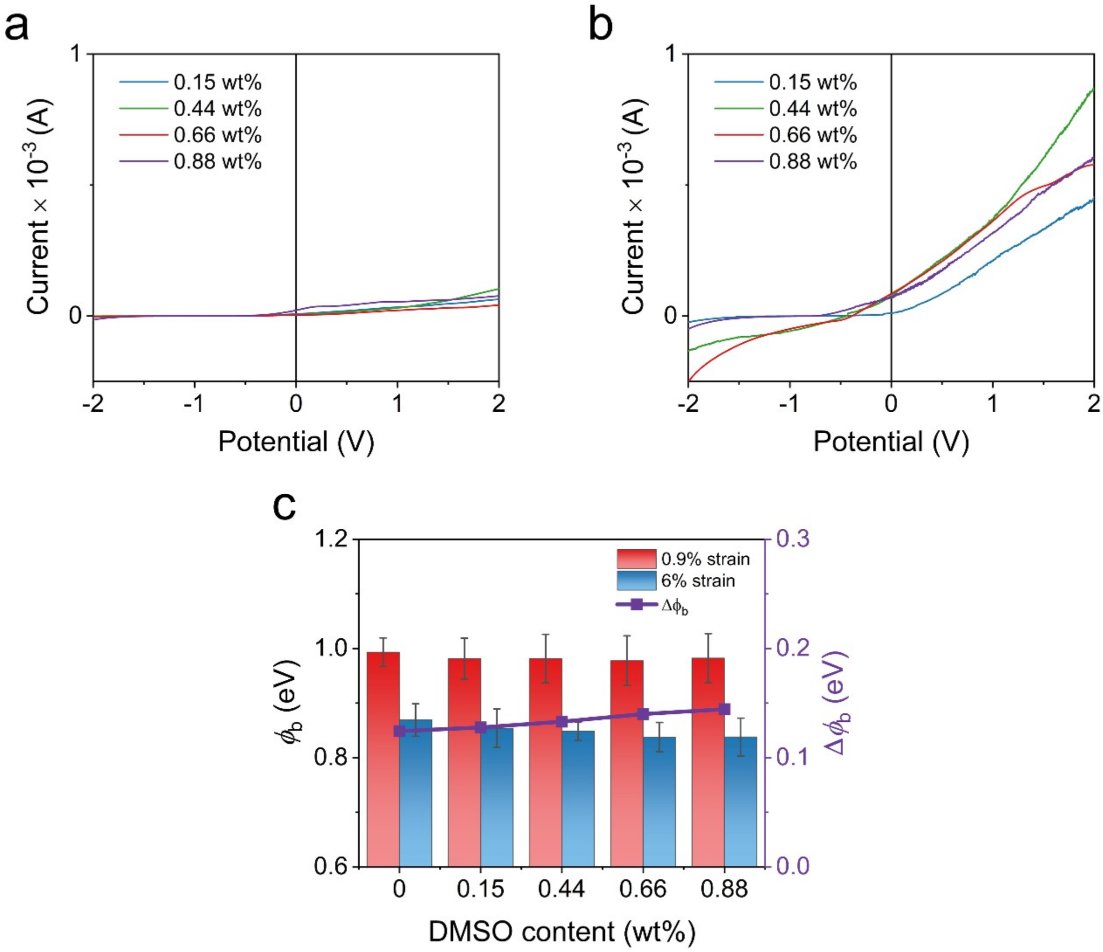

Fig. S19 I–V curves of the PPy-DMSO devices at the strain levels of (a) 0.9% and (b) 6.0%. (c) Calculated Schottky barrier height under compression and without compression (relative humidity: 70%, temperature: 20 °C).

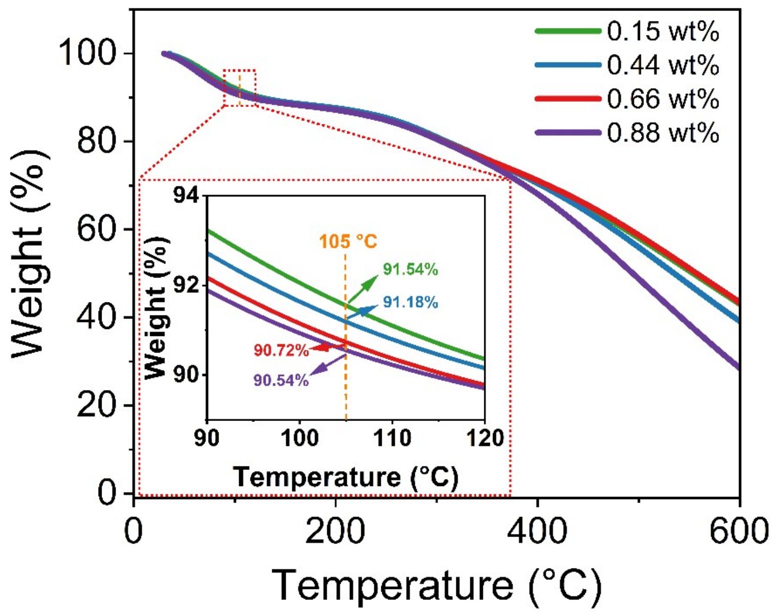

Fig. S20 TGA curves for PPy-DMSO samples after being stored at 70% RH for one week.

The PPy with different DMSO contents showed slightly different water contents, being 8.46 wt%, 8.82 wt%, 9.28 wt%, and 9.46 wt% when PPy contained 0.15 wt%, 0.44 wt%, 0.66 wt%, and 0.88 wt% DMSO, respectively.

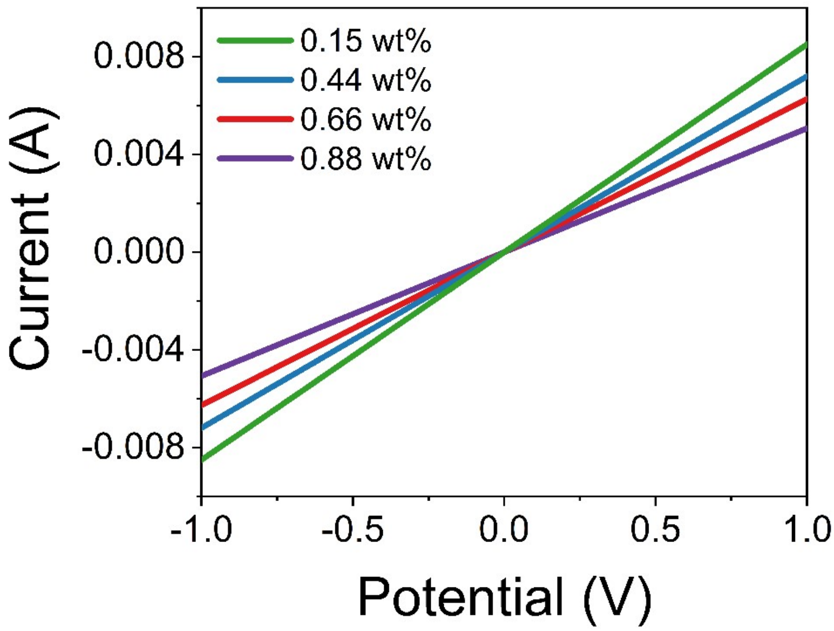

Fig. S21 I–V characteristics of the Au/PPy-DMSO/Au at the strain 6.0% (relative humidity: 70%, temperature: 20 °C).

The resistance of the PPy-DMSO discs is 117.51 Ω, 138.89 Ω, 159.49 Ω, and 197.24 Ω for the PPy containing 0.15 wt%, 0.44 wt%, 0.66 wt%, and 0.88 wt% DMSO, respectively.

a

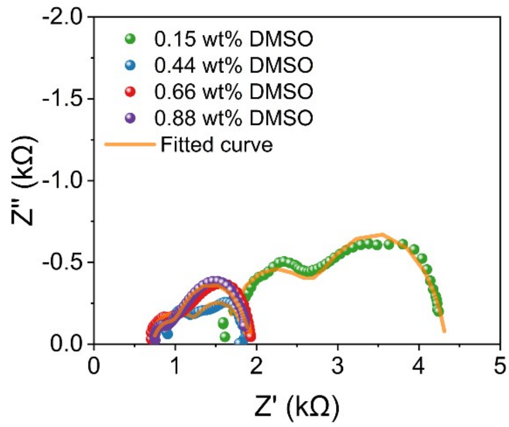

b

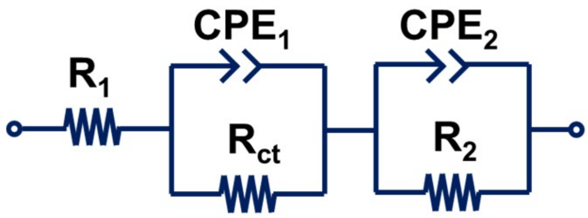

c

DMSO content (wt%)	R_1 (kΩ)	CPE_1 (μF)	R_{ct} (kΩ)	CPE_2 (μF)	R_2 (kΩ)
0.15	1.599	2.841E-3	1.633	1.118E-5	1.105
0.44	0.867	2.613E-4	0.710	2.883E-3	0.317
0.66	0.667	2.683E-2	0.799	2.568E-6	0.478
0.88	0.724	3.674E-3	0.927	3.883E-5	0.277

Fig. S22 (a) Nyquist plots and (b) equivalent circuit of PPy-based devices doped with different DMSO content within the frequency region of 1MHz to 100 Hz. (c) The fitted values of equivalent circuits (Chi-square was below 0.01).

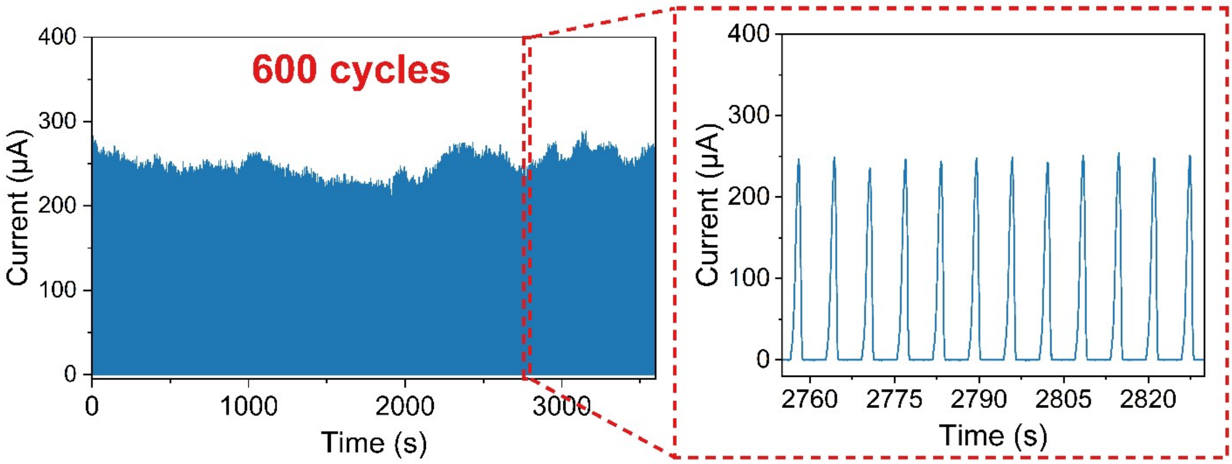

Fig. S23 Current output stability test result for the PPy-DMSO device (DMSO content: 0.66 wt%, cycles: 600 times, strain 6%, compressing & releasing speed: 0.035mm s^{-1}, relative humidity: 70%, temperature: 20 °C).

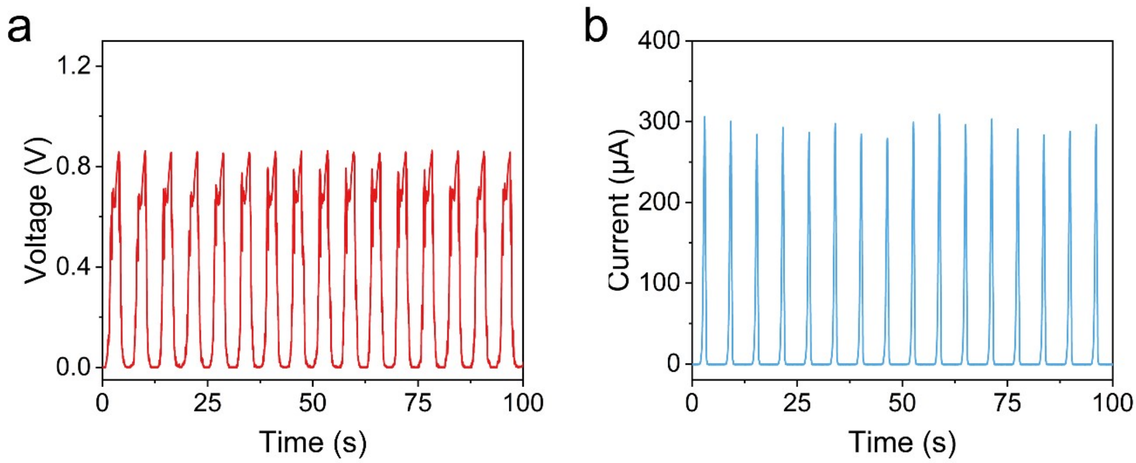

Fig. S24 (a) voltage and (b) current outputs of PPy-DMSO devices using the PPy-DMSO (post-treatment method, strain: 6%, compressing & releasing speed: 0.035mm s^{-1}, relative humidity: 70% RH, temperature: 20 °C).

PPy-DMSO was prepared by a post-treatment method. 20 ml 15 wt% DMSO was mixed with 5.0 g PPy powder. After 3 hours of stirring at room temperature, the powder was filtered out and dried at 65 degrees for 24 hours. The dry powder was compressed into a disc and stored at 70% RH, 20 °C, for one week.

Supplementary Video

Video S1: A video to show the lighting of a commercial LED powered by Schottky devices made of PPy-DMSO.

References

1 S. Lin, Y. Lu, S. Feng, Z. Hao and Y. Yan, *Adv. Mater.*, 2019, **31**, 1804398.

2 Y. Lu, Z. Hao, S. Feng, R. Shen, Y. Yan and S. Lin, *iScience*, 2019, **22**, 58–69.

3 J. Liu, A. Goswami, K. Jiang, F. Khan, S. Kim, R. McGee, Z. Li, Z. Hu, J. Lee and T. Thundat, *Nat. Nanotechnol.*, 2018, **13**, 112–116.

4 V. A. Sharov, P. A. Alekseev, M. S. Dunaevskiy, R. R. Reznik and G. E. Cirlin, *J. Phys. Conf. Ser.*, 2019, **1400**, 66055.

5 S. Ferrie, N. Darwish, J. J. Gooding and S. Ciampi, *Nano Energy*, 2020, **78**, 105210.

6 J. Liu, M. I. Cheikh, R. Bao, H. Peng, F. Liu, Z. Li, K. Jiang, J. Chen and T. Thundat, *Adv. Electron. Mater.*, 2019, **5**, 1900464.

7 R. Xu, Q. Zhang, J. Y. Wang, D. Liu, J. Wang and Z. L. Wang, *Nano Energy*, 2019, **66**, 104185.

8 J. Liu, F. Liu, R. Bao, K. Jiang, F. Khan, Z. Li, H. Peng, J. Chen, A. Alodhayb and T. Thundat, *ACS Appl. Mater. Interfaces*, 2019, **11**, 35404–35409.

9 H. Shao, J. Fang, H. Wang, L. Dai and T. Lin, *Adv. Mater.*, 2016, **28**, 1461–1466.

10 H. Shao, J. Fang, H. Wang, H. Zhou and T. Lin, *J. Mater. Chem. A*, 2017, **5**, 8267–8273.

11 H. Shao, J. Fang, H. Wang, H. Niu, H. Zhou, Y. Cao, F. Chen, S. Fu and T. Lin, *Nano Energy*, 2019, **62**, 171–180.

12 X. Ding, H. Shao, H. Wang, W. Yang, J. Fang, D. Zhang and T. Lin, *Nano Energy*, 2021, **89**, 106367.

13 W. Sun, N. Wang, J. Li, S. Xu, L. Song, Y. Liu and D. Wang, *Electrochim. Acta*, 2021, **391**, 138994.

14 Q. Zhou, K. Lee, K. N. Kim, J. G. Park, J. Pan, J. Bae, J. M. Baik and T. Kim, *Nano Energy*, 2019, **57**, 903–910.

15 D. Liu, J. Liu, M. Yang, N. Cui, H. Wang, L. Gu, L. Wang and Y. Qin, *Nano Energy*, 2021, **88**, 106303.

16 S. Yan, J. Lu, W. Song and R. Xiao, *Nano Energy*, 2018, **48**, 248–255.

17 J. Shen, Z. Li, J. Yu and B. Ding, *Nano Energy*, 2017, **40**, 282–288.

18 Y.-T. Jao, P.-K. Yang, C.-M. Chiu, Y.-J. Lin, S.-W. Chen, D. Choi and Z.-H. Lin, *Nano Energy*, 2018, **50**, 513–520.

19 H. Guo, J. Chen, L. Tian, Q. Leng, Y. Xi and C. Hu, *ACS Appl. Mater. Interfaces*, 2014, **6**, 17184–17189.

20 F. Ejehi, R. Mohammadpour, E. Asadian, P. Sasanpour, S. Fardindoost and O. Akhavan, *Sci. Rep.*, 2020, **10**, 1–11.

21 J. Chen, P. He, T. Huang, D. Zhang, G. Wang, S. Yang, X. Xie and G. Ding, *Nano Energy*, 2021, **90**, 106593.

22 Y. Hu, X. Wang, H. Li, H. Li and Z. Li, *Nano Energy*, 2020, **71**, 104640.

23 W. Zang, W. Wang, D. Zhu, L. Xing and X. Xue, *RSC Adv.*, 2014, **4**, 56211–56215.

24 D. Zhu, Y. Fu, W. Zang, Y. Zhao, L. Xing and X. Xue, *Sensors Actuators B Chem.*, 2014, **205**, 12–19.